

Plane-wave scattering by an ellipsoid composed of an orthorhombic dielectric-magnetic material with arbitrarily oriented constitutive principal axes

Hamad M. Alkhoori

Department of Electrical Engineering, The Pennsylvania State University, University Park, Pennsylvania
16802, USA

Akhlesh Lakhtakia

Department of Engineering Science and Mechanics, The Pennsylvania State University, University Park,
Pennsylvania 16802, USA

James K. Breakall

Department of Electrical Engineering, The Pennsylvania State University, University Park, Pennsylvania
16802, USA

Craig F. Bohren

Department of Meteorology, The Pennsylvania State University, University Park, Pennsylvania 16802, USA

Abstract

The extended boundary condition method can be formulated to study plane-wave scattering by an ellipsoid composed of an orthorhombic dielectric-magnetic material whose relative permittivity dyadic is a scalar multiple of its relative permeability dyadic, when the constitutive principal axes are arbitrarily oriented with respect to the shape principal axes. Known vector spherical wavefunctions are used to represent the fields in the surrounding matter-free space. After deriving closed-form expressions for the vector spherical wavefunctions for the scattering material, the internal fields are represented as superpositions of those vector spherical wavefunctions. The unknown scattered-field coefficients are related to the known incident-field coefficients by a transition matrix. The total scattering and absorption efficiencies are highly affected by the orientation of the constitutive principal axes relative to the shape principal axes, and the effect of the orientational mismatch between the two sets of principal axes is more pronounced as the electrical size increases. The dependence of the total scattering efficiency, but not of the absorption efficiency, on the angle of rotation about a shape principal axis can be predicted qualitatively from the variation of a scalar function with respect to the angle of rotation. The total scattering and absorption efficiencies do not depend on the polarization state of incident plane wave when the scattering material is impedance-matched to free space. The polarization state of the incident plane wave has a more discernible effect on the total scattering and absorption efficiencies for ellipsoids compared to spheres.

1 Introduction

Analysis of frequency-domain electromagnetic fields in a homogeneous dielectric-magnetic material require the specification of two constitutive dyadics, one of which relates $\mathbf{D}(\mathbf{r})$ to $\mathbf{E}(\mathbf{r})$ and the other relates $\mathbf{B}(\mathbf{r})$ to $\mathbf{H}(\mathbf{r})$. Each constitutive dyadic comprises nine complex components in general [1, 2]. It is convenient to choose a coordinate system in which at least one of the two constitutive dyadics is diagonal [3, 4]. Any symmetric dyadic can be diagonalized, and diagonalization can be effected through a rotation of axes in some situations [5]. Rotation transforms a problem from a laboratory coordinate system into a coordinate system in which a constitutive dyadic is diagonal. The eigenvalues of a diagonal dyadic populate its diagonal and the corresponding eigenvectors determine the principal axes of that dyadic.

Obtaining closed-form expressions for the electromagnetic field phasors in a homogeneous dielectric-magnetic material is generally difficult, all the more so if Cartesian coordinates are not used [3, 6]. Recently, however, closed-form expressions of vector spherical wavefunctions were obtained for an orthorhombic dielectric-magnetic material whose relative permittivity dyadic is a scalar multiple of its relative permeability dyadic [7]. These wavefunctions were used to formulate a scattering problem wherein an incident field impinges on an object composed of the chosen material and suspended in free space (i.e., vacuum). The formulation is based on the extended boundary condition method (EBCM), also called the null-field method and the T-matrix method [8, 9]. This method requires knowledge of (i) the bilinear expansions of the dyadic Green functions for free space [10, 11] and (ii) the vector wavefunctions to completely express the field phasors induced inside the object.

The frequency-domain constitutive relations of the chosen material are [7]

$$\mathbf{D}(\mathbf{r}) = \varepsilon_0 \varepsilon_r \underline{\underline{C}} \cdot \mathbf{E}(\mathbf{r}) \quad (1)$$

and

$$\mathbf{B}(\mathbf{r}) = \mu_0 \mu_r \underline{\underline{C}} \cdot \mathbf{H}(\mathbf{r}), \quad (2)$$

where ε_0 and μ_0 are the permittivity and permeability of free space, respectively; ε_r and μ_r are complex functions of the angular frequency ω ; and the dyadic

$$\underline{\underline{C}} = \underline{\underline{S}} \cdot \underline{\underline{A}} \cdot \underline{\underline{A}} \cdot \underline{\underline{S}}^{-1}. \quad (3)$$

Here,

$$\underline{\underline{S}} = \underline{\underline{R}}_z(\gamma) \cdot \underline{\underline{R}}_y(\beta) \cdot \underline{\underline{R}}_z(\alpha) \quad (4)$$

is a product of three rotation dyadics, with

$$\begin{aligned} \underline{\underline{R}}_z(\zeta) &= (\hat{\mathbf{x}}\hat{\mathbf{x}} + \hat{\mathbf{y}}\hat{\mathbf{y}}) \cos \zeta - (\hat{\mathbf{x}}\hat{\mathbf{y}} - \hat{\mathbf{y}}\hat{\mathbf{x}}) \sin \zeta + \hat{\mathbf{z}}\hat{\mathbf{z}}, \\ \zeta &\in \{\alpha, \gamma\}, \end{aligned} \quad (5)$$

and

$$\underline{\underline{R}}_y(\beta) = (\hat{\mathbf{x}}\hat{\mathbf{x}} + \hat{\mathbf{z}}\hat{\mathbf{z}}) \cos \beta - (\hat{\mathbf{z}}\hat{\mathbf{x}} - \hat{\mathbf{x}}\hat{\mathbf{z}}) \sin \beta + \hat{\mathbf{y}}\hat{\mathbf{y}}. \quad (6)$$

The dyadic $\underline{\underline{R}}_z(\alpha)$ represents a rotation by $\alpha \in [0, \pi]$ around the z axis, $\underline{\underline{R}}_y(\beta)$ represents a rotation by $\beta \in [0, \pi]$ around the y axis, and $\underline{\underline{R}}_z(\gamma)$ represents a rotation by $\gamma \in [0, \pi]$ around the z axis.

The diagonal dyadic $\underline{\underline{A}}$ is defined as

$$\underline{\underline{A}} = \alpha_x^{-1} \hat{\mathbf{x}}\hat{\mathbf{x}} + \alpha_y^{-1} \hat{\mathbf{y}}\hat{\mathbf{y}} + \hat{\mathbf{z}}\hat{\mathbf{z}}. \quad (7)$$

The constitutive-anisotropy parameters α_x and α_y are real positive functions of ω to ensure that $\underline{\underline{A}}$ is positive definite [12], which allows for an affine transformation of space wherein fields can be compactly expressed [7]. By virtue of Eqs. (1)–(7), the permittivity dyadic $\underline{\underline{\varepsilon}} = \varepsilon_0 \varepsilon_r \underline{\underline{C}}$ and the permeability dyadic $\underline{\underline{\mu}} = \mu_0 \mu_r \underline{\underline{C}}$ have the same set of three principal axes.

In addition to the constitutive principal axes, an object has a shape. The ellipsoidal shape is convex and possesses three principal axes. In a coordinate system with its origin at the centroid of an ellipsoid, the surface \mathcal{S} of that ellipsoid is delineated by the position vector

$$\begin{aligned} \mathbf{r}_s(\theta, \phi) &= c \underline{\underline{U}} \cdot [(\hat{\mathbf{x}} \cos \phi + \hat{\mathbf{y}} \sin \phi) \sin \theta + \hat{\mathbf{z}} \cos \theta], \\ \theta &\in [0, \pi], \quad \phi \in [0, 2\pi]. \end{aligned} \quad (8)$$

The shape dyadic

$$\underline{\underline{U}} = (a \hat{\mathbf{x}}\hat{\mathbf{x}} + b \hat{\mathbf{y}}\hat{\mathbf{y}}) / c + \hat{\mathbf{z}}\hat{\mathbf{z}} \quad (9)$$

contains the x , y , and z axes as the shape principal axes of an ellipsoid with linear dimensions $2a$, $2b$, and $2c$ along those axes. We take the laboratory coordinate system to be the one in which the shape dyadic $\underline{\underline{U}}$ is defined via Eq. (9).

Whether or not materials described by Eqs. (1)–(7) exist in nature, an effectively homogeneous material described by those equations can potentially be fabricated by properly dispersing electrically small wires, loops, and other inclusions of different materials and shapes in some host material [13, 14, 15, 16]. Also, certain spacetime metrics can yield the chosen forms of $\underline{\underline{\varepsilon}}$ and $\underline{\underline{\mu}}$ [17].

In this paper, we consider scattering by an ellipsoid endowed with the shape dyadic $\underline{\underline{U}}$, the permittivity dyadic $\underline{\underline{\varepsilon}}$ and the permeability dyadic $\underline{\underline{\mu}}$. The scattering characteristics must depend on the orientation of the

constitutive principal axes determined from $\underline{\underline{C}}$ relative to the orientation of shape principal axes determined from $\underline{\underline{U}}$. In order to distinguish the effects of the orientation of the shape principal axes from those of the orientation of the constitutive principal axes, comparison with a sphere composed of the same material is necessary.

Solution of the boundary-value problem of scattering requires closed-form expressions of the vector spherical wavefunctions in the laboratory coordinate system, but these are available [7] only for $\underline{\underline{S}} = \underline{\underline{I}}$, the identity dyadic [3]. Therefore, we derived the expressions for $\underline{\underline{S}} \neq \underline{\underline{I}}$. In order to quantify the effects of orienting the constitutive principal axes differently from the shape principal axes, we computed the total scattering efficiency when the ellipsoid is illuminated by a plane wave [18, 19].

This paper is organized as follows. The closed-form expressions of the vector spherical wavefunctions in the laboratory coordinate system are presented in Sec. 2 for the material specified by Eqs. (1)–(7). In the same section, we also solve the scattering problem using the EBCM. In Section 3, we present and analyze computed values of the total scattering efficiency in relation to the orientations of the constitutive principal axes and shape principal axes. Our conclusions are summarized in Section 4.

An $\exp(-i\omega t)$ dependence on time t is implicit throughout the analysis with $i = \sqrt{-1}$. Vectors are in boldface, unit vectors are decorated by caret, dyadics are double underlined, and column vectors as well as matrices are enclosed in square brackets. The free-space wavenumber is denoted by $k_0 = \omega\sqrt{\mu_0\varepsilon_0}$ and the intrinsic impedance of free space by $\eta_0 = \sqrt{\mu_0/\varepsilon_0}$. We define the relative impedance $\eta_r = \sqrt{\mu_r/\varepsilon_r}$ and the wavenumber $k = k_0\sqrt{\varepsilon_r}\sqrt{\mu_r}\alpha_x^{-1}\alpha_y^{-1}$.

2 Theory

2.1 Closed-form expressions of vector spherical wavefunctions

On substituting Eqs. (1) and (2) into the source-free Maxwell curl equations $\nabla \times \mathbf{E}(\mathbf{r}) = i\omega\mathbf{B}(\mathbf{r})$ and $\nabla \times \mathbf{H}(\mathbf{r}) = -i\omega\mathbf{D}(\mathbf{r})$, one obtains

$$\left. \begin{aligned} \nabla \times \mathbf{E}(\mathbf{r}) &= i\omega[\mu_0\mu_r\underline{\underline{S}} \cdot \underline{\underline{A}} \cdot \underline{\underline{A}} \cdot \underline{\underline{S}}^{-1} \cdot \mathbf{H}(\mathbf{r})] \\ \nabla \times \mathbf{H}(\mathbf{r}) &= -i\omega[\varepsilon_0\varepsilon_r\underline{\underline{S}} \cdot \underline{\underline{A}} \cdot \underline{\underline{A}} \cdot \underline{\underline{S}}^{-1} \cdot \mathbf{E}(\mathbf{r})] \end{aligned} \right\} \quad (10)$$

The complete solutions $\mathbf{E}(\mathbf{r})$ and $\mathbf{H}(\mathbf{r})$ of Eqs. (10) can be written as superposition of vector spherical wavefunctions

$$\mathfrak{M}_{smn}^{(j)}(\mathbf{r}) = \underline{\underline{S}} \cdot \underline{\underline{A}}^{-1} \cdot \mathbf{M}_{smn}^{(j)}(k\underline{\underline{A}}^{-1} \cdot \underline{\underline{S}} \cdot \mathbf{r}) \quad (11)$$

and

$$\mathfrak{N}_{smn}^{(j)}(\mathbf{r}) = \underline{\underline{S}} \cdot \underline{\underline{A}}^{-1} \cdot \mathbf{N}_{smn}^{(j)}(k\underline{\underline{A}}^{-1} \cdot \underline{\underline{S}} \cdot \mathbf{r}), \quad (12)$$

as proved elsewhere [7, 20].

Standard texts [10, 18, 21] contain closed-form expressions of $\mathbf{M}_{smn}^{(j)}(k\mathbf{r})$ and $\mathbf{N}_{smn}^{(j)}(k\mathbf{r})$ in spherical coordinates. Whereas $\mathbf{M}_{smn}^{(1)}(k\mathbf{r})$ and $\mathbf{N}_{smn}^{(1)}(k\mathbf{r})$ are regular at the origin $r = 0$, $\mathbf{M}_{smn}^{(3)}(k\mathbf{r})$ and $\mathbf{N}_{smn}^{(3)}(k\mathbf{r})$ are regular as $r \rightarrow \infty$. The index n denotes the order of the spherical Bessel function $j_n(kr)$ for $j = 1$, and of the spherical Hankel functions $h_n^{(1)}(kr)$ for $j = 3$, appearing in these wavefunctions. Furthermore, these wavefunctions involve the associated Legendre function $P_n^m(\cos\theta)$ of order n and degree m , and the index s stands for either even (e) or odd (o) parity.

Closed-form expressions of the wavefunctions $\mathbf{M}_{smn}^{(j)}(k\underline{\underline{A}}^{-1} \cdot \mathbf{r})$ and $\mathbf{N}_{smn}^{(j)}(k\underline{\underline{A}}^{-1} \cdot \mathbf{r})$ are also available [7]. But those of $\mathbf{M}_{smn}^{(j)}(k\underline{\underline{A}}^{-1} \cdot \underline{\underline{S}} \cdot \mathbf{r})$ and $\mathbf{N}_{smn}^{(j)}(k\underline{\underline{A}}^{-1} \cdot \underline{\underline{S}} \cdot \mathbf{r})$ had to be derived for the work reported in this paper.

Let $\mathbf{r} \equiv (x, y, z) \equiv (r, \theta, \phi)$ and $\mathbf{r}'' \equiv (x'', y'', z'') \equiv (r'', \theta'', \phi'')$ where

$$\mathbf{r}'' = \underline{\underline{A}}^{-1} \cdot \underline{\underline{S}} \cdot \mathbf{r}. \quad (13)$$

After expressing (r'', θ'', ϕ'') in terms of (r, θ, ϕ) , as well as $(\hat{\mathbf{r}}'', \hat{\boldsymbol{\theta}}'', \hat{\boldsymbol{\phi}}'')$ in terms of $(\hat{\mathbf{r}}, \hat{\boldsymbol{\theta}}, \hat{\boldsymbol{\phi}})$, one obtains

$$\begin{aligned} \mathfrak{M}_{smn}^{(j)}(\mathbf{r}) = & \underline{\underline{R}}_{cs}^T(\theta, \phi) \cdot \underline{\underline{S}} \cdot \underline{\underline{A}}^{-1} \cdot \underline{\underline{R}}_{cs}(\theta, \phi) \cdot \left(\mathfrak{J}_n^{(j)}(k\mathbf{r}) \{ \hat{\mathbf{r}} [t_{21}(\theta, \phi) \mathcal{Q}_{smn}(\theta, \phi) - t_{31}(\theta, \phi) \mathcal{R}_{smn}(\theta, \phi)] \right. \\ & \left. + \hat{\boldsymbol{\theta}} [t_{22}(\theta, \phi) \mathcal{Q}_{smn}(\theta, \phi) - t_{32}(\theta, \phi) \mathcal{R}_{smn}(\theta, \phi)] + \hat{\boldsymbol{\phi}} [t_{23}(\theta, \phi) \mathcal{Q}_{smn}(\theta, \phi) - t_{33}(\theta, \phi) \mathcal{R}_{smn}(\theta, \phi)] \right), \end{aligned} \quad (14)$$

and

$$\begin{aligned} \mathfrak{N}_{smn}^{(j)}(\mathbf{r}) = & \underline{\underline{R}}_{cs}^T(\theta, \phi) \cdot \underline{\underline{S}} \cdot \underline{\underline{A}}^{-1} \cdot \underline{\underline{R}}_{cs}(\theta, \phi) \cdot \\ & \left(\hat{\mathbf{r}} \left\{ t_{11}(\theta, \phi) \frac{\mathfrak{J}_n^{(j)}(k\mathbf{r})}{kr g_1(\theta, \phi)} \mathcal{P}_{smn}(\theta, \phi) + \mathfrak{K}_n^{(j)}(k\mathbf{r}) [t_{21}(\theta, \phi) \mathcal{R}_{smn}(\theta, \phi) + t_{31}(\theta, \phi) \mathcal{Q}_{smn}(\theta, \phi)] \right\} \right. \\ & + \hat{\boldsymbol{\theta}} \left\{ t_{12}(\theta, \phi) \frac{\mathfrak{J}_n^{(j)}(k\mathbf{r})}{kr g_1(\theta, \phi)} \mathcal{P}_{smn}(\theta, \phi) + \mathfrak{K}_n^{(j)}(k\mathbf{r}) [t_{22}(\theta, \phi) \mathcal{R}_{smn}(\theta, \phi) + t_{32}(\theta, \phi) \mathcal{Q}_{smn}(\theta, \phi)] \right\} \\ & \left. + \hat{\boldsymbol{\phi}} \left\{ t_{13}(\theta, \phi) \frac{\mathfrak{J}_n^{(j)}(k\mathbf{r})}{kr g_1(\theta, \phi)} \mathcal{P}_{smn}(\theta, \phi) + \mathfrak{K}_n^{(j)}(k\mathbf{r}) [t_{23}(\theta, \phi) \mathcal{R}_{smn}(\theta, \phi) + t_{33}(\theta, \phi) \mathcal{Q}_{smn}(\theta, \phi)] \right\} \right), \end{aligned} \quad (15)$$

where the superscript T denotes the transpose,

$$\underline{\underline{R}}_{cs}(\theta, \phi) = \begin{pmatrix} \sin \theta \cos \phi & \cos \theta \cos \phi & -\sin \phi \\ \sin \theta \sin \phi & \cos \theta \sin \phi & \cos \phi \\ \cos \theta & -\sin \theta & 0 \end{pmatrix}, \quad (16)$$

$$\begin{aligned} t_{11}(\theta, \phi) = & \frac{1}{g_1(\theta, \phi)} [g_2(\theta, \phi)(S_{32} \sin \theta \sin \phi + S_{31} \sin \theta \cos \phi + S_{33} \cos \theta) + g_4(\theta, \phi)(S_{12} \sin \theta \sin \phi + S_{11} \sin \theta \cos \phi \\ & + S_{13} \cos \theta) + g_5(\theta, \phi)(S_{22} \sin \theta \sin \phi + S_{21} \sin \theta \cos \phi + S_{23} \cos \theta)], \end{aligned} \quad (17)$$

$$\begin{aligned} t_{12}(\theta, \phi) = & \frac{1}{g_1(\theta, \phi)} [g_2(\theta, \phi)(S_{31} \cos \theta \cos \phi + S_{32} \cos \theta \sin \phi - S_{33} \sin \theta) + g_4(\theta, \phi)(S_{11} \cos \theta \cos \phi + S_{12} \cos \theta \sin \phi \\ & - S_{13} \sin \theta) + g_5(\theta, \phi)(S_{21} \cos \theta \cos \phi + S_{22} \cos \theta \sin \phi - S_{23} \sin \theta)], \end{aligned} \quad (18)$$

$$\begin{aligned} t_{13}(\theta, \phi) = & \frac{1}{g_1(\theta, \phi)} [-g_4(\theta, \phi)(S_{11} \sin \phi - S_{12} \cos \phi) + g_5(\theta, \phi)(S_{22} \cos \phi - S_{21} \sin \phi) + g_2(\theta, \phi)(S_{32} \cos \phi - S_{31} \sin \phi)], \end{aligned} \quad (19)$$

$$\begin{aligned} t_{21}(\theta, \phi) = & \frac{1}{g_1(\theta, \phi) g_3(\theta, \phi)} \{ g_2(\theta, \phi) [g_4(\theta, \phi)(S_{12} \sin \theta \sin \phi + S_{11} \sin \theta \cos \phi + S_{13} \cos \theta) + g_5(\theta, \phi)(S_{22} \sin \theta \sin \phi \\ & + S_{21} \sin \theta \cos \phi + S_{23} \cos \theta)] - g_3^2(\theta, \phi)(S_{32} \sin \theta \sin \phi + S_{31} \sin \theta \cos \phi + S_{33} \cos \theta) \}, \end{aligned} \quad (20)$$

$$\begin{aligned} t_{22}(\theta, \phi) = & \frac{1}{g_1(\theta, \phi) g_3(\theta, \phi)} \{ g_2(\theta, \phi) [g_4(\theta, \phi)(S_{11} \cos \theta \cos \phi + S_{12} \cos \theta \sin \phi - S_{13} \sin \theta) + g_5(\theta, \phi)(S_{21} \cos \theta \cos \phi \\ & + S_{22} \cos \theta \sin \phi - S_{23} \sin \theta)] - g_3^2(\theta, \phi)(S_{31} \cos \theta \cos \phi + S_{32} \cos \theta \sin \phi - S_{33} \sin \theta) \}, \end{aligned} \quad (21)$$

$$\begin{aligned} t_{23}(\theta, \phi) = & \frac{1}{g_1(\theta, \phi) g_3(\theta, \phi)} \{ g_2(\theta, \phi) [g_5(\theta, \phi)(S_{22} \cos \phi - S_{21} \sin \phi) - g_4(\theta, \phi)(S_{11} \sin \phi - S_{12} \cos \phi)] \\ & + g_3^2(\theta, \phi)(S_{31} \sin \phi - S_{32} \cos \phi) \}, \end{aligned} \quad (22)$$

$$\begin{aligned} t_{31}(\theta, \phi) = & \frac{1}{g_3(\theta, \phi)} [g_4(\theta, \phi)(S_{22} \sin \theta \sin \phi + S_{21} \sin \theta \cos \phi + S_{23} \cos \theta) - g_5(\theta, \phi)(S_{12} \sin \theta \sin \phi + S_{11} \sin \theta \cos \phi \\ & + S_{13} \cos \theta)], \end{aligned} \quad (23)$$

$$t_{32}(\theta, \phi) = \frac{1}{g_3(\theta, \phi)} [g_4(\theta, \phi)(S_{21} \cos \theta \cos \phi + S_{22} \cos \theta \sin \phi - S_{23} \sin \theta) - g_5(\theta, \phi)(S_{11} \cos \theta \cos \phi + S_{12} \cos \theta \sin \phi - S_{13} \sin \theta)], \quad (24)$$

and

$$t_{33}(\theta, \phi) = \frac{1}{g_3(\theta, \phi)} [g_5(\theta, \phi)(S_{11} \sin \phi - S_{12} \cos \phi) + g_4(\theta, \phi)(S_{22} \cos \phi - S_{21} \sin \phi)]. \quad (25)$$

In the foregoing expressions, $S_{\nu\nu'}$, $\nu \in [1, 3]$ and $\nu' \in [1, 3]$, are elements of the dyadic $\underline{\underline{S}}$ written in matrix form as

$$\underline{\underline{S}} = \begin{pmatrix} \cos \gamma \cos \beta \cos \alpha - \sin \gamma \sin \alpha & -\sin \gamma \cos \beta \cos \alpha - \cos \gamma \sin \alpha & \sin \beta \cos \alpha \\ \cos \gamma \cos \beta \sin \alpha + \sin \gamma \cos \alpha & -\sin \gamma \cos \beta \sin \alpha + \cos \gamma \cos \alpha & \sin \beta \sin \alpha \\ -\cos \gamma \sin \beta & \sin \gamma \sin \beta & \cos \beta \end{pmatrix}. \quad (26)$$

Furthermore,

$$\mathfrak{J}_n^{(j)}(k\mathbf{r}) = z_n[kr g_1(\theta, \phi)], \quad (27)$$

$$\mathfrak{K}_n(k\mathbf{r}) = \frac{n+1}{kr g_1(\theta, \phi)} \mathfrak{J}_n^{(j)}(k\mathbf{r}) - \mathfrak{J}_{n+1}^{(j)}(k\mathbf{r}), \quad (28)$$

$$\mathcal{Q}_{smn}(\theta, \phi) = \mathcal{Q}_{mn}(\theta, \phi) \mathcal{U}_{sm}(\theta, \phi), \quad (29)$$

$$\mathcal{R}_{smn}(\theta, \phi) = \mathcal{R}_{mn}(\theta, \phi) \mathcal{V}_{sm}(\theta, \phi), \quad (30)$$

$$\mathcal{P}_{smn}(\theta, \phi) = \mathcal{P}_{mn}(\theta, \phi) \mathcal{V}_{sm}(\theta, \phi), \quad (31)$$

$$\mathcal{Q}_{mn}(\theta, \phi) = \frac{m g_1(\theta, \phi)}{g_3(\theta, \phi)} P_n^m \begin{bmatrix} g_2(\theta, \phi) \\ g_1(\theta, \phi) \end{bmatrix}, \quad (32)$$

$$\mathcal{P}_{mn}(\theta, \phi) = n(n+1) P_n^m \begin{bmatrix} g_2(\theta, \phi) \\ g_1(\theta, \phi) \end{bmatrix}, \quad (33)$$

$$\mathcal{R}_{mn}(\theta, \phi) = \frac{g_1(\theta, \phi)}{g_3(\theta, \phi)} \left\{ (n-m+1) P_{n+1}^m \begin{bmatrix} g_2(\theta, \phi) \\ g_1(\theta, \phi) \end{bmatrix} - (n+1) \frac{g_2(\theta, \phi)}{g_1(\theta, \phi)} P_n^m \begin{bmatrix} g_2(\theta, \phi) \\ g_1(\theta, \phi) \end{bmatrix} \right\}, \quad (34)$$

$$\mathcal{U}_{sm}(\theta, \phi) = \begin{Bmatrix} -\sin [mg_6(\theta, \phi)] \\ \cos [mg_6(\theta, \phi)] \end{Bmatrix}, \quad s = \begin{Bmatrix} e \\ o \end{Bmatrix}, \quad (35)$$

and

$$\mathcal{V}_{sm}(\theta, \phi) = \begin{Bmatrix} \cos [mg_6(\theta, \phi)] \\ \sin [mg_6(\theta, \phi)] \end{Bmatrix}, \quad s = \begin{Bmatrix} e \\ o \end{Bmatrix}, \quad (36)$$

where $z_n(\cdot)$ is either $j_n(\cdot)$ when $j = 1$, or $h_n^{(1)}(\cdot)$ when $j = 3$. In Eqs. (17)-(25) and (27)-(36), the following angular functions have been used:

$$g_1(\theta, \phi) = \left\{ [g_2(\theta, \phi)]^2 + [g_3(\theta, \phi)]^2 \right\}^{1/2}, \quad (37)$$

$$g_2(\theta, \phi) = \cos \beta \cos \theta - \sin \beta \sin \theta \cos(\alpha + \phi), \quad (38)$$

$$g_3(\theta, \phi) = \left\{ [g_4(\theta, \phi)]^2 + [g_5(\theta, \phi)]^2 \right\}^{1/2}, \quad (39)$$

$$g_4(\theta, \phi) = \alpha_x \left\{ \cos \gamma [\cos \beta \sin \theta \cos(\alpha + \phi) + \sin \beta \cos \theta] - \sin \gamma \sin \theta \sin(\alpha + \phi) \right\}, \quad (40)$$

$$g_5(\theta, \phi) = \alpha_y \left\{ \sin \gamma [\cos \beta \sin \theta \cos(\alpha + \phi) + \sin \beta \cos \theta] + \cos \gamma \sin \theta \sin(\alpha + \phi) \right\}, \quad (41)$$

and

$$g_6(\theta, \phi) = \tan^{-1} \left[\frac{g_5(\theta, \phi)}{g_4(\theta, \phi)} \right]. \quad (42)$$

2.2 EBCM equations

Consider an ellipsoid fully occupying the region V . Thus, $\mathbf{r}(\theta, \phi) \in V \Rightarrow |\mathbf{r}(\theta, \phi)| \leq |\mathbf{r}_S(\theta, \phi)|$. The region outside V is vacuous. With the stipulation that the source of the incident electromagnetic field lies outside the sphere circumscribing V [9], the incident electric field phasor may be written as

$$\mathbf{E}_{\text{inc}}(\mathbf{r}) = \lim_{N \rightarrow \infty} \sum_{s \in \{e, o\}} \sum_{n=1}^N \sum_{m=0}^n \left\{ D_{mn} [A_{smn}^{(1)} \mathbf{M}_{smn}^{(1)}(k_0 \mathbf{r}) + B_{smn}^{(1)} \mathbf{N}_{smn}^{(1)}(k_0 \mathbf{r})] \right\}, \quad (43)$$

where the normalization factor

$$D_{mn} = (2 - \delta_{m0}) \frac{(2n+1)(n-m)!}{4n(n+1)(n+m)!} \quad (44)$$

involves the Kronecker delta $\delta_{mm'}$ and the expansion coefficients $A_{smn}^{(1)}$ and $B_{smn}^{(1)}$ are supposed to be known $\forall \{s, m, n\}$.

Likewise, the scattered electric field phasor outside the sphere circumscribing V can be expanded as

$$\mathbf{E}_{\text{sca}}(\mathbf{r}) = \lim_{N \rightarrow \infty} \sum_{s \in \{e, o\}} \sum_{n=1}^N \sum_{m=0}^n \left\{ D_{mn} [A_{smn}^{(3)} \mathbf{M}_{smn}^{(3)}(k_0 \mathbf{r}) + B_{smn}^{(3)} \mathbf{N}_{smn}^{(3)}(k_0 \mathbf{r})] \right\}, \quad (45)$$

where the expansion coefficients $A_{smn}^{(3)}$ and $B_{smn}^{(3)}$ are not known.

Inside V , the electric and magnetic field phasors are represented by a superposition of the vector spherical wavefunctions derived in Sec. 2.2.1 as

$$\mathbf{E}_{\text{int}}(\mathbf{r}) = \lim_{N \rightarrow \infty} \sum_{s \in \{e, o\}} \sum_{n=1}^N \sum_{m=0}^n \left[b_{smn} \mathfrak{M}_{smn}^{(1)}(\mathbf{r}) + c_{smn} \mathfrak{N}_{smn}^{(1)}(\mathbf{r}) \right] \quad (46)$$

and

$$\mathbf{H}_{\text{int}}(\mathbf{r}) = -\frac{i}{\eta_0 \eta_r} \lim_{N \rightarrow \infty} \sum_{s \in \{e, o\}} \sum_{n=1}^N \sum_{m=0}^n \left[b_{smn} \mathfrak{N}_{smn}^{(1)}(\mathbf{r}) + c_{smn} \mathfrak{M}_{smn}^{(1)}(\mathbf{r}) \right], \quad (47)$$

where the expansion coefficients b_{smn} and c_{smn} are not known.

On (i) making use of the Ewald-Oseen extinction theorem and the Huygens principle, (ii) exploiting the orthogonality properties of $\mathbf{M}_{smn}^{(j)}(k_0 \mathbf{r})$ and $\mathbf{N}_{smn}^{(j)}(k_0 \mathbf{r})$ on a unit sphere [7], and (iii) application of the continuity of tangential electric and magnetic fields across S , a matrix relation emerges between the incident field and scattered field coefficients [8, 9]. This relation is written compactly as

$$\begin{bmatrix} [A^{(3)}] \\ [B^{(3)}] \end{bmatrix} = [T] \begin{bmatrix} [A^{(1)}] \\ [B^{(1)}] \end{bmatrix}, \quad (48)$$

where the column vectors $[A^{(j)}]$ and $[B^{(j)}]$ contain the coefficients $A_{smn}^{(j)}$ and $B_{smn}^{(j)}$, respectively.

The matrix

$$[T] = -[Y^{(3)}][Y^{(1)}]^{-1} \quad (49)$$

is called the transition matrix or the T matrix. The matrix $[Y^{(j)}]$, $j \in [1, 3]$, is symbolically written as

$$[Y^{(j)}] = \left(\begin{array}{c|c} I_{smn,s'm'n'}^{(j)} & J_{smn,s'm'n'}^{(j)} \\ \hline K_{smn,s'm'n'}^{(j)} & L_{smn,s'm'n'}^{(j)} \end{array} \right). \quad (50)$$

The matrix elements in Eq. (50) are double integrals given by

$$\begin{aligned} I_{smn,s'm'n'}^{(j)} = & -\frac{ik_0^2}{\pi} \iint_{\mathcal{S}} d^2r_s \\ & \left[\left\{ \mathbf{N}_{smn}^{(\ell)}(k_0\mathbf{r}_s) \cdot \left[\hat{\mathbf{n}}(\mathbf{r}_s) \times \mathfrak{M}_{s'm'n'}^{(1)}(\mathbf{r}_s) \right] \right\} \right. \\ & \left. + \eta_r^{-1} \left\{ \mathbf{M}_{smn}^{(\ell)}(k_0\mathbf{r}_s) \cdot \left[\hat{\mathbf{n}}(\mathbf{r}_s) \times \mathfrak{N}_{s'm'n'}^{(1)}(\mathbf{r}_s) \right] \right\} \right] \end{aligned} \quad (51)$$

$$\begin{aligned} J_{smn,s'm'n'}^{(j)} = & -\frac{ik_0^2}{\pi} \iint_{\mathcal{S}} d^2r_s \\ & \left[\left\{ \mathbf{N}_{smn}^{(\ell)}(k_0\mathbf{r}_s) \cdot \left[\hat{\mathbf{n}}(\mathbf{r}_s) \times \mathfrak{N}_{s'm'n'}^{(1)}(\mathbf{r}_s) \right] \right\} \right. \\ & \left. + \eta_r^{-1} \left\{ \mathbf{M}_{smn}^{(\ell)}(k_0\mathbf{r}_s) \cdot \left[\hat{\mathbf{n}}(\mathbf{r}_s) \times \mathfrak{M}_{s'm'n'}^{(1)}(\mathbf{r}_s) \right] \right\} \right] \end{aligned} \quad (52)$$

$$\begin{aligned} K_{smn,s'm'n'}^{(j)} = & -\frac{ik_0^2}{\pi} \iint_{\mathcal{S}} d^2r_s \\ & \left[\left\{ \mathbf{M}_{smn}^{(\ell)}(k_0\mathbf{r}_s) \cdot \left[\hat{\mathbf{n}}(\mathbf{r}_s) \times \mathfrak{M}_{s'm'n'}^{(1)}(\mathbf{r}_s) \right] \right\} \right. \\ & \left. + \eta_r^{-1} \left\{ \mathbf{N}_{smn}^{(\ell)}(k_0\mathbf{r}_s) \cdot \left[\hat{\mathbf{n}}(\mathbf{r}_s) \times \mathfrak{N}_{s'm'n'}^{(1)}(\mathbf{r}_s) \right] \right\} \right] \end{aligned} \quad (53)$$

and

$$\begin{aligned} L_{smn,s'm'n'}^{(j)} = & -\frac{ik_0^2}{\pi} \iint_{\mathcal{S}} d^2r_s \\ & \left[\left\{ \mathbf{M}_{smn}^{(\ell)}(k_0\mathbf{r}_s) \cdot \left[\hat{\mathbf{n}}(\mathbf{r}_s) \times \mathfrak{N}_{s'm'n'}^{(1)}(\mathbf{r}_s) \right] \right\} \right. \\ & \left. + \eta_r^{-1} \left\{ \mathbf{N}_{smn}^{(\ell)}(k_0\mathbf{r}_s) \cdot \left[\hat{\mathbf{n}}(\mathbf{r}_s) \times \mathfrak{M}_{s'm'n'}^{(1)}(\mathbf{r}_s) \right] \right\} \right] \end{aligned} \quad (54)$$

In the foregoing double integrals, $\hat{\mathbf{n}}(\mathbf{r}_s)$ is the unit outward normal to \mathcal{S} at $\mathbf{r}_s \in \mathcal{S}$ and $\ell = j+2(\text{mod}4) \in [3, 1]$.

2.3 Plane-wave incidence

Consider a plane wave incident on the ellipsoid such that

$$\mathbf{E}_{\text{inc}}(\mathbf{r}) = \hat{\mathbf{e}}_{\text{inc}} \exp(ik_0\hat{\mathbf{k}}_{\text{inc}} \cdot \mathbf{r}), \quad (55)$$

where the unit vector

$$\hat{\mathbf{k}}_{\text{inc}} = (\hat{\mathbf{x}} \sin \theta_{\text{inc}} \cos \phi_{\text{inc}} + \hat{\mathbf{y}} \sin \theta_{\text{inc}} \sin \phi_{\text{inc}} + \hat{\mathbf{z}} \cos \theta_{\text{inc}}) \quad (56)$$

contains the angles $\theta_{\text{inc}} \in [0, \pi]$ and $\phi_{\text{inc}} \in [0, 2\pi)$ that together define the incidence direction.

The unit vector $\hat{\mathbf{e}}_{\text{inc}}$ defines the polarization state, with the stipulation that $\hat{\mathbf{k}}_{\text{inc}} \cdot \hat{\mathbf{e}}_{\text{inc}} = 0$. For any specific choice of $\hat{\mathbf{k}}_{\text{inc}}$, a choice has to be made for $\hat{\mathbf{e}}_{\text{inc}}$. If this choice is denoted by $\hat{\mathbf{e}}_{\text{inc}}^{(1)}$, the second choice becomes automatic: $\hat{\mathbf{e}}_{\text{inc}}^{(2)} = \hat{\mathbf{k}}_{\text{inc}} \times \hat{\mathbf{e}}_{\text{inc}}^{(1)}$. Thus,

$$\hat{\mathbf{e}}_{\text{inc}}^{\parallel} = \hat{\mathbf{x}} \cos \theta_{\text{inc}} \cos \phi_{\text{inc}} + \hat{\mathbf{y}} \cos \theta_{\text{inc}} \sin \phi_{\text{inc}} - \hat{\mathbf{z}} \sin \theta_{\text{inc}} \quad (57)$$

and

$$\hat{\mathbf{e}}_{\text{inc}}^{\perp} = -\hat{\mathbf{x}} \sin \phi_{\text{inc}} + \hat{\mathbf{y}} \cos \phi_{\text{inc}} \quad (58)$$

represent the parallel and perpendicular polarization states, respectively; likewise,

$$\hat{\mathbf{e}}_{\text{inc}}^{\text{LCP}} = \frac{1}{\sqrt{2}} \left(\hat{\mathbf{e}}_{\text{inc}}^{\parallel} + i \hat{\mathbf{e}}_{\text{inc}}^{\perp} \right) \quad (59)$$

and

$$\hat{\mathbf{e}}_{\text{inc}}^{\text{RCP}} = \frac{1}{\sqrt{2}} \left(\hat{\mathbf{e}}_{\text{inc}}^{\parallel} - i \hat{\mathbf{e}}_{\text{inc}}^{\perp} \right), \quad (60)$$

respectively, represent the left-circular and right-circular polarization (LCP and RCP) states.

The expansion coefficients on the right side of Eq. (43) are given by [10, 19]

$$\left. \begin{aligned} A_{smn}^{(1)} &= 4i^n \sqrt{n(n+1)} \hat{\mathbf{e}}_{\text{inc}} \cdot \mathbf{C}_{smn}(\theta_{\text{inc}}, \phi_{\text{inc}}) \\ B_{smn}^{(1)} &= 4i^{n-1} \sqrt{n(n+1)} \hat{\mathbf{e}}_{\text{inc}} \cdot [\hat{\mathbf{k}}_{\text{inc}} \times \mathbf{C}_{smn}(\theta_{\text{inc}}, \phi_{\text{inc}})] \end{aligned} \right\}, \quad (61)$$

where the vector spherical harmonic

$$\begin{aligned} \mathbf{C}_{smn}(\theta, \phi) &= \frac{1}{\sqrt{n(n+1)}} \left[\mp m \frac{P_n^m(\cos \theta)}{\sin \theta} \begin{Bmatrix} \sin(m\phi) \\ \cos(m\phi) \end{Bmatrix} \hat{\boldsymbol{\theta}} \right. \\ &\quad \left. - \frac{dP_n^m(\cos \theta)}{d\theta} \begin{Bmatrix} \cos(m\phi) \\ \sin(m\phi) \end{Bmatrix} \hat{\boldsymbol{\phi}} \right], \quad s = \begin{Bmatrix} e \\ o \end{Bmatrix}. \end{aligned} \quad (62)$$

Let the expansion coefficients $A_{smn}^{(1)\parallel}$ and $B_{smn}^{(1)\parallel}$ represent the incident parallel-polarized plane wave, whereas the expansion coefficients $A_{smn}^{(1)\perp}$ and $B_{smn}^{(1)\perp}$ the incident perpendicularly polarized plane wave. Then, the twin relations

$$A_{smn}^{(1)\parallel} = i B_{smn}^{(1)\perp}, \quad B_{smn}^{(1)\parallel} = i A_{smn}^{(1)\perp} \quad (63)$$

emerge from Eqs. (57), (58), and (61).

Let the expansion coefficients $A_{smn}^{(1)\text{L}}$ and $B_{smn}^{(1)\text{L}}$ represent the incident LCP plane wave, whereas $A_{smn}^{(1)\text{R}}$ and $B_{smn}^{(1)\text{R}}$ represent the incident RCP plane wave. Then,

$$\left. \begin{aligned} A_{smn}^{(1)\text{L}} &= \frac{1}{\sqrt{2}} \left(A_{smn}^{(1)\parallel} + i A_{smn}^{(1)\perp} \right) \\ B_{smn}^{(1)\text{L}} &= \frac{1}{\sqrt{2}} \left(B_{smn}^{(1)\parallel} + i B_{smn}^{(1)\perp} \right) \end{aligned} \right\} \quad (64)$$

and

$$\left. \begin{aligned} A_{smn}^{(1)\text{R}} &= \frac{1}{\sqrt{2}} \left(A_{smn}^{(1)\parallel} - i A_{smn}^{(1)\perp} \right) \\ B_{smn}^{(1)\text{R}} &= \frac{1}{\sqrt{2}} \left(B_{smn}^{(1)\parallel} - i B_{smn}^{(1)\perp} \right) \end{aligned} \right\}, \quad (65)$$

follow from Eqs. (59) and (60). Using Eqs. (63) in the foregoing relations finally yields the twin relations

$$A_{smn}^{(1)\text{L}} = B_{smn}^{(1)\text{L}}, \quad A_{smn}^{(1)\text{R}} = -B_{smn}^{(1)\text{R}} \quad (66)$$

2.4 Total scattering, extinction, and absorption efficiencies

In the far zone, the scattered electric field phasor can be approximated as [22, 18]

$$\mathbf{E}_{\text{sca}}(r, \theta, \phi) \approx \mathbf{F}_{\text{sca}}(\theta, \phi) \exp(ik_0 r)/r \quad (67)$$

where [19]

$$\mathbf{F}_{\text{sca}}(\theta, \phi) = (1/k_0) \lim_{N \rightarrow \infty} \sum_{s \in \{e, o\}} \sum_{n=1}^N \sum_{m=0}^n \left\{ (-i)^n D_{mn} \sqrt{n(n+1)} \right. \\ \left. \left[-iA_{smn}^{(3)} \underline{\mathbf{I}} + B_{smn}^{(3)} \hat{\mathbf{r}} \times \underline{\mathbf{I}} \right] \cdot \mathbf{C}_{smn}(\theta, \phi) \right\}. \quad (68)$$

The differential scattering efficiency is defined as

$$Q_D(\theta, \phi) = (4/c^2) |\mathbf{F}_{\text{sca}}(\theta, \phi)|^2. \quad (69)$$

Upon integrating $Q_D(\theta, \phi)$ over the entire solid angle, the total scattering efficiency is obtained as

$$Q_{\text{sca}} = (k_0 c)^{-2} \\ \times \lim_{N \rightarrow \infty} \sum_{s \in \{e, o\}} \sum_{n=1}^N \sum_{m=0}^n D_{mn} \left[|A_{smn}^{(3)}|^2 + |B_{smn}^{(3)}|^2 \right]. \quad (70)$$

By virtue of the forward-scattering theorem [23, 24], the extinction efficiency can be calculated as

$$Q_{\text{ext}} = (4/k_0 c^2) \text{Im} [\mathbf{F}_{\text{sca}}(\theta_{\text{inc}}, \phi_{\text{inc}}) \cdot \hat{\mathbf{e}}_{\text{inc}}^*], \quad (71)$$

where the asterisk denotes the complex conjugate. Substitution of Eqs. (61) and (68) on the right side of Eq. (71) yields

$$Q_{\text{ext}} = (k_0 c)^{-2} \\ \times \lim_{N \rightarrow \infty} \sum_{s \in \{e, o\}} \sum_{n=1}^N \sum_{m=0}^n D_{mn} \text{Re} \left[-A_{smn}^{(3)} A_{smn}^{(1)*} + B_{smn}^{(3)} B_{smn}^{(1)*} \right]. \quad (72)$$

The absorption efficiency can then be calculated as

$$Q_{\text{abs}} = Q_{\text{ext}} - Q_{\text{sca}}. \quad (73)$$

The scattered field coefficients $A_{smn}^{(3)\parallel}$ and $B_{smn}^{(3)\parallel}$ are related to the incident field coefficients $A_{smn}^{(1)\parallel}$ and $B_{smn}^{(1)\parallel}$, and so on, through Eq. (48). Accordingly,

$$\left. \begin{aligned} A_{smn}^{(3)\text{L}} &= \frac{1}{\sqrt{2}} \left(A_{smn}^{(3)\parallel} + iA_{smn}^{(3)\perp} \right) \\ B_{smn}^{(3)\text{L}} &= \frac{1}{\sqrt{2}} \left(B_{smn}^{(3)\parallel} + iB_{smn}^{(3)\perp} \right) \end{aligned} \right\} \quad (74)$$

and

$$\left. \begin{aligned} A_{smn}^{(3)\text{R}} &= \frac{1}{\sqrt{2}} \left(A_{smn}^{(3)\parallel} - iA_{smn}^{(3)\perp} \right) \\ B_{smn}^{(3)\text{R}} &= \frac{1}{\sqrt{2}} \left(B_{smn}^{(3)\parallel} - iB_{smn}^{(3)\perp} \right) \end{aligned} \right\}. \quad (75)$$

Equations (70), (71), and (73) then deliver the identities

$$\left. \begin{aligned} Q_{\text{sca}}^{\text{L}} + Q_{\text{sca}}^{\text{R}} &= Q_{\text{sca}}^{\parallel} + Q_{\text{sca}}^{\perp} \\ Q_{\text{ext}}^{\text{L}} + Q_{\text{ext}}^{\text{R}} &= Q_{\text{ext}}^{\parallel} + Q_{\text{ext}}^{\perp} \\ Q_{\text{abs}}^{\text{L}} + Q_{\text{abs}}^{\text{R}} &= Q_{\text{abs}}^{\parallel} + Q_{\text{abs}}^{\perp} \end{aligned} \right\}. \quad (76)$$

These identities hold regardless of the composition of the scattering material, so long as it is linear.

Table 1: Adequate value of N and computation time on a Dell Alienware 18 laptop computer to determine Q_b and Q_{sca} for a sphere or an ellipsoid ($a/c = 1/2$ and $b/c = 2/3$), when $\varepsilon_r = 2$, $\mu_r = 1.05$, $k_0c = 3$, $\theta_{\text{inc}} = 45^\circ$, $\phi_{\text{inc}} = 30^\circ$, and $\hat{\mathbf{e}}_{\text{inc}} = \hat{\mathbf{e}}_{\text{inc}}^{\parallel}$.

Object	Anisotropy parameters	Orientation angles	N	Computation time (s)
Ellipsoid	$\alpha_x = 1.2, \alpha_y = 1.1$	$\alpha = 20^\circ, \beta = 40^\circ, \gamma = 30^\circ$	8	8940.44
Ellipsoid	$\alpha_x = 1.2, \alpha_y = 1.1$	$\alpha = \beta = \gamma = 0^\circ$	7	4991.35
Ellipsoid	$\alpha_x = \alpha_y = 1$	$\alpha = \beta = \gamma = 0^\circ$	6	2617.74
Sphere	$\alpha_x = 1.2, \alpha_y = 1.1$	$\alpha = 20^\circ, \beta = 40^\circ, \gamma = 30^\circ$	7	6408.86
Sphere	$\alpha_x = 1.2, \alpha_y = 1.1$	$\alpha = \beta = \gamma = 0^\circ$	6	3034.59
Sphere	$\alpha_x = \alpha_y = 1$	$\alpha = \beta = \gamma = 0^\circ$	5	1593.66
Sphere (using symmetries of double integrals)	$\alpha_x = \alpha_y = 1$	$\alpha = \beta = \gamma = 0^\circ$	5	56.94

2.5 Impedance-matched scattering material

When $\eta_r = 1$, i.e., $\varepsilon_r = \mu_r$, the material chosen for the scatterer can be said to be impedance matched to free space. The equalities $I_{smn,s'm'n'}^{(j)} = L_{smn,s'm'n'}^{(j)}$ and $J_{smn,s'm'n'}^{(j)} = K_{smn,s'm'n'}^{(j)}$ then follow from Eqs. (51)-(54). In consequence, if the column vectors $[A^{(1)}]$ and $[B^{(1)}]$ on the right side of Eq. (48) were to be interchanged, then the column vectors $[A^{(3)}]$ and $[B^{(3)}]$ on the right side of Eq. (48) shall have to be interchanged as well; both $Q_D(\theta, \phi)$ and Q_{sca} would remain unaffected because $\hat{\mathbf{r}} \cdot \mathbf{C}_{smn}(\theta, \phi) \equiv 0$ [25]. Consequently, both $Q_D(\theta, \phi)$ and Q_{sca} do not depend on the polarization state of the incident plane wave. Additional analysis [25] shows that Q_{abs} and Q_{ext} also do not depend on the polarization state of the incident plane wave.

3 Numerical Results and Discussion

The T matrix was computed on the MathematicaTM version 11.3 platform implemented on a Dell Alienware 18 laptop computer with 16 GB memory. We used the Gauss–Legendre quadrature scheme [26] to evaluate the integrals in Eqs. (51)-(54). By testing against known integrals [27] so as to compute integrals correct to $\pm 0.1\%$ relative error, the number of nodes was chosen to be 24 for integration over θ as well as for integration over ϕ . The computation of the inverse of $[Y^{(1)}]$ was carried out using the lower-upper decomposition method [28]. The value of N was incremented by unity until the backscattering efficiency $Q_b = Q_D(-\hat{\mathbf{k}}_{\text{inc}})$ converged within a tolerance of $\pm 0.1\%$.

Validation of the program was accomplished by comparing with results available for simpler problems, such as Lorenz–Mie theory for isotropic dielectric/magnetic/dielectric-magnetic spheres [21, 18]. For a sphere as well as for an ellipsoid composed of a material described by Eqs. (1)–(7) with $\underline{\underline{S}} = \underline{\underline{I}}$, our program was completely in accord with published data [29, 30, 19].

Anisotropy considerably enhances computational requirements, as summarized in Table 1. For example, $N = 7$ is needed for a sphere ($a/c = b/c = 1$) and $N = 8$ for an ellipsoid ($a/c = 1/2$ and $b/c = 2/3$), when we choose $\varepsilon_r = 2$, $\mu_r = 1.05$, $\alpha_x = 1.2$, $\alpha_y = 1.1$, $\alpha = 20^\circ$, $\beta = 40^\circ$, $\gamma = 30^\circ$, $k_0c = 3$, $\theta_{\text{inc}} = 45^\circ$, and $\phi_{\text{inc}} = 30^\circ$. Because ε_r and μ_r are both real, we exploited the relation $[Y^{(3)}] = \text{Re}[Y^{(1)}]$ in order to reduce computation time. When we set $\alpha = \beta = \gamma = 0^\circ$ so that the constitutive principal axes coincide with the shape principal axes, $N = 6$ is needed for the sphere and $N = 7$ for the ellipsoid. However, we need $N = 5$ and $N = 6$ for the sphere and the ellipsoid, respectively, when we eliminate anisotropy by setting $\alpha_x = \alpha_y = 1$.

Another way to appreciate the enhancement of computational requirements by anisotropy is to examine the computation time. According to Table 1, anisotropy doubles the computation time even when the constitutive principal axes coincide with the shape principal axes; the computation time increases significantly

when the two sets of principal axes do not coincide. Incidentally, the double integrals defined in Eqs. (51)–(54) simply considerably for an isotropic dielectric-magnetic spheroid [31] due to rotational symmetry about the z axis (i.e., r_s is independent of ϕ), and even more simplification occurs for an isotropic dielectric-magnetic sphere because $r_s = c$ then for all values of θ and ϕ in Eq. (8). When incorporated in a computer program, such simplifications greatly reduce the computation time, as can be deduced by comparing the last two rows of Table 1. Also, we note that concurrent computation of a substantial number of double integrals using multiple processors in parallel will reduce the computation time.

Now, we present numerical results on the total scattering efficiency of a biaxial dielectric-magnetic ellipsoid in relation to

- the propagation direction $\hat{\mathbf{k}}_{\text{inc}}$ of the incident plane wave;
- the polarization state of the incident plane wave ($\hat{\mathbf{e}}_{\text{inc}}$);
- the constitutive-anisotropy parameters α_x and α_y ;
- the nonsphericity parameters a/c and b/c ;
- the orientation angles α , β , and γ ; and
- the electrical length k_0c .

Comparison is made to analogous numerical results for a biaxial dielectric-magnetic spheroid and a biaxial dielectric-magnetic sphere.

3.1 Orientational mismatch of $\underline{\underline{C}}$ and $\underline{\underline{U}}$

In order to illustrate the effects of the lack of coincidence of the principal axes of $\underline{\underline{C}}$ and $\underline{\underline{U}}$, Fig. 1 shows plots of $Q_{\text{sca}}^{\parallel}$, Q_{sca}^{\perp} , $Q_{\text{sca}}^{\text{L}}$, and $Q_{\text{sca}}^{\text{R}}$ vs. $k_0c \in [0, 3]$ for a biaxially dielectric-magnetic ellipsoid, described by $\varepsilon_r = 2$, $\mu_r = 1.05$, $\alpha_x = 1.2$, $\alpha_y = 1.1$, $a/c = 1/2$, and $b/c = 2/3$. The incidence direction is specified by $\theta_{\text{inc}} = 45^\circ$ and $\phi_{\text{inc}} = 30^\circ$. Since the scattering material is non-dissipative, $Q_{\text{abs}} \equiv 0$ for all polarization states of the incident plane wave.

Figure 1(a) depicts plots of $Q_{\text{sca}}^{\parallel}$, Q_{sca}^{\perp} , $Q_{\text{sca}}^{\text{L}}$, and $Q_{\text{sca}}^{\text{R}}$ vs. k_0c when the principal axes of $\underline{\underline{C}}$ and $\underline{\underline{U}}$ coincide, i.e., $\alpha = \beta = \gamma = 0^\circ$. We see that $Q_{\text{sca}}^{\parallel} > Q_{\text{sca}}^{\perp}$ regardless of $k_0c \in [0, 3]$. Furthermore, $Q_{\text{sca}}^{\text{L}} \simeq Q_{\text{sca}}^{\text{R}}$, so that Q_{sca} for either circularly polarized plane wave is almost the arithmetic mean of $Q_{\text{sca}}^{\parallel}$ and Q_{sca}^{\perp} by virtue of Eq. (76)₁.

Rotation of $\underline{\underline{C}}$ about the z axis of the laboratory coordinate system has a small but noticeable effect on Q_{sca} , as becomes evident from comparing Fig. 1(a) with Fig. 1(b), the latter being drawn for $\alpha = 20^\circ$ and $\beta = \gamma = 0^\circ$. A subsequent rotation by $\beta = 40^\circ$ about the new y axis also affects Q_{sca} , regardless of the polarization state of the incident plane wave; see Fig. 1(c) drawn for $\alpha = 20^\circ$, $\beta = 30^\circ$, and $\gamma = 0^\circ$. The final rotation by $\gamma = 30^\circ$ about the latest z axis also has an effect on Q_{sca} in Fig. 1(d), regardless of the polarization state of the incident plane wave and the electrical size of the ellipsoid. In all panels of Fig. 1, for the most part Q_{sca} increases as k_0c does. The excess of $Q_{\text{sca}}^{\text{R}}$ over $Q_{\text{sca}}^{\text{L}}$ is clearer in Figs. 1(c,d) than in Figs. 1(a,b).

Figure 2 depicts plots of Q_{sca} vs. k_0c for the same biaxially dielectric-magnetic ellipsoid of Fig. 1, except that $\varepsilon_r = \mu_r = 2$. Since the scattering material is impedance matched to the surrounding free space, Q_{sca} is independent of $\hat{\mathbf{e}}_{\text{inc}}$ as discussed in Sec. 2.2.5. The effect of orientational mismatch of $\underline{\underline{C}}$ and $\underline{\underline{U}}$ as k_0c increases is readily apparent in this figure, and the effects of various rotations are exactly the same as those reported for Fig. 1.

Next, we consider scattering materials with:

- (a) $\varepsilon_r \mu_r < 0 \Rightarrow \{\varepsilon_r \geq 0, \mu_r \leq 0\}$ and
- (b) $\varepsilon_r \mu_r > 0 \Rightarrow \{\varepsilon_r \geq 0, \mu_r \geq 0\}$,

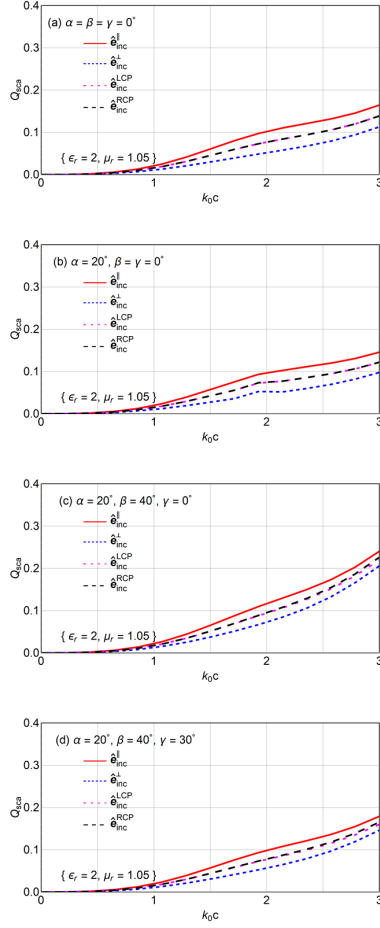


Figure 1: $Q_{\text{sca}}^{\parallel}$, Q_{sca}^{\perp} , $Q_{\text{sca}}^{\text{L}}$, and $Q_{\text{sca}}^{\text{R}}$ vs. $k_0c \in [0, 3]$ for a biaxially dielectric-magnetic ellipsoid described by $\varepsilon_r = 2$, $\mu_r = 1.05$, $\alpha_x = 1.2$, $\alpha_y = 1.1$, $a/c = 1/2$, and $b/c = 2/3$. The angles of incidence are $\theta_{\text{inc}} = 45^\circ$ and $\phi_{\text{inc}} = 30^\circ$. (a) $\alpha = \beta = \gamma = 0^\circ$; (b) $\alpha = 20^\circ$ and $\beta = \gamma = 0^\circ$; (c) $\alpha = 20^\circ$, $\beta = 40^\circ$, and $\gamma = 0^\circ$; and (d) $\alpha = 20^\circ$, $\beta = 40^\circ$, and $\gamma = 30^\circ$.

both ε_r and μ_r being purely real. Simultaneous reversal of the signs of ε_r and μ_r in case (a) changes neither the relative wavenumber k/k_0 nor the relative impedance η_r of the scattering material; hence, that reversal should not have any effect on the scattered electric and magnetic field phasors. Simultaneous reversal of the signs of ε_r and μ_r in case (b) does not change η_r but k/k_0 does change; hence, that reversal should affect the scattered field phasors.

Figure 3(a) shows plots of $Q_{\text{sca}}^{\parallel}$, Q_{sca}^{\perp} , $Q_{\text{sca}}^{\text{L}}$, and $Q_{\text{sca}}^{\text{R}}$ vs. k_0c for the biaxially dielectric-magnetic ellipsoid of Fig. 1(d), except that either $\{\varepsilon_r = 2, \mu_r = -1.05\}$ or $\{\varepsilon_r = -2, \mu_r = 1.05\}$. As predicted in the previous paragraph, the plots for $\{\varepsilon_r = 2, \mu_r = -1.05\}$ and $\{\varepsilon_r = -2, \mu_r = 1.05\}$ are identical, and these plots differ from those for $\{\varepsilon_r = 2, \mu_r = 1.05\}$. Furthermore, Q_{sca} increases with k_0c in Fig. 3(a) regardless of the polarization state of the incident plane wave, but a similar trend is not followed strictly in Fig. 1(d).

Figure 3(b) shows plots of $Q_{\text{sca}}^{\parallel}$, Q_{sca}^{\perp} , $Q_{\text{sca}}^{\text{L}}$, and $Q_{\text{sca}}^{\text{R}}$ vs. k_0c for the biaxially dielectric-magnetic ellipsoid of Fig. 1(d), except that $\{\varepsilon_r = -2, \mu_r = -1.05\}$. Again, as predicted two paragraphs previously, the plots for $\{\varepsilon_r = -2, \mu_r = -1.05\}$ are not the same as for $\{\varepsilon_r = 2, \mu_r = 1.05\}$. Also, regardless of the polarization state of the incident plane wave, Q_{sca} has a complicated dependence on k_0c in Fig. 3(b), but for the most

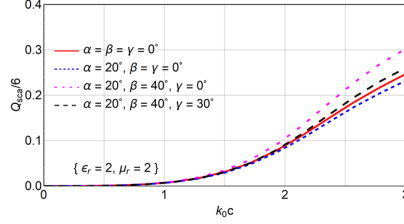


Figure 2: Q_{sca} vs. $k_0 c \in [0, 3]$ for a biaxially dielectric-magnetic ellipsoid described by $\varepsilon_r = \mu_r = 2$, $\alpha_x = 1.2$, $\alpha_y = 1.1$, $a/c = 1/2$, and $b/c = 2/3$. The angles of incidence are $\theta_{\text{inc}} = 45^\circ$ and $\phi_{\text{inc}} = 30^\circ$.

part Q_{sca} increases with $k_0 c$ in Fig. 1(d). Compared to ellipsoids characterized by either $\{\varepsilon_r > 0, \mu_r > 0\}$ or $\{\varepsilon_r \geq 0, \mu_r \leq 0\}$, the difference between $Q_{\text{sca}}^{\text{R}}$ and $Q_{\text{sca}}^{\text{L}}$ is much more pronounced for the ellipsoid characterized by $\{\varepsilon_r < 0, \mu_r < 0\}$.

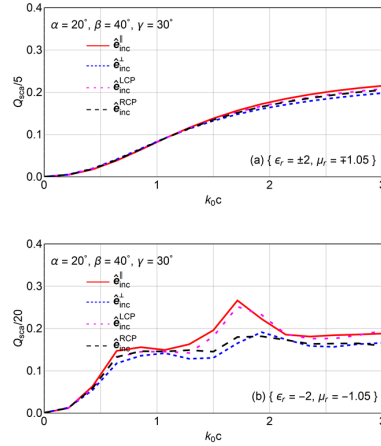


Figure 3: $Q_{\text{sca}}^{\parallel}$, Q_{sca}^{\perp} , $Q_{\text{sca}}^{\text{L}}$, and $Q_{\text{sca}}^{\text{R}}$ vs. $k_0 c \in [0, 3]$ for a biaxially dielectric-magnetic ellipsoid when $\alpha_x = 1.2$, $\alpha_y = 1.1$, $\alpha = 20^\circ$, $\beta = 40^\circ$, and $\gamma = 30^\circ$, $a/c = 1/2$, and $b/c = 2/3$. The angles of incidence are $\theta_{\text{inc}} = 45^\circ$ and $\phi_{\text{inc}} = 30^\circ$. (a) $\varepsilon_r = \pm 2$ and $\mu_r = \mp 1.05$, (b) $\varepsilon_r = -2$, and $\mu_r = -1.05$.

Suppose that $|\varepsilon_r|$, $|\mu_r|$, and $k_0 c$ are fixed. Then, for a fixed polarization state of the incident plane wave, Q_{sca} is maximum for $\{\varepsilon_r < 0, \mu_r < 0\}$, intermediate for $\{\varepsilon_r \geq 0, \mu_r \leq 0\}$, and minimum for $\{\varepsilon_r > 0, \mu_r > 0\}$, according to Figs. 1(d) and 3(a,b). Calculations for several other values of $|\varepsilon_r|$ and $|\mu_r|$ are in agreement with this conclusion.

Finally, in this section we consider the effect of dissipation in the scattering material. The calculations for Fig. 1 were repeated but with $\varepsilon_r = 2 + i0.1$ and $\mu_r = 1.05 + i0.01$; accordingly, $Q_{\text{abs}} \neq 0$. As dissipation depressed Q_{sca} slightly but did not otherwise alter the conclusions drawn from Fig. 1, plots of $Q_{\text{sca}}^{\parallel}$, Q_{sca}^{\perp} , $Q_{\text{sca}}^{\text{L}}$, and $Q_{\text{sca}}^{\text{R}}$ vs. $k_0 c$ are not presented here.

Figure 4 contains plots of $Q_{\text{abs}}^{\parallel}$, Q_{abs}^{\perp} , $Q_{\text{abs}}^{\text{L}}$, and $Q_{\text{abs}}^{\text{R}}$ vs. $k_0 c \in [0, 3]$. When the principal axes of $\underline{\underline{C}}$ and $\underline{\underline{U}}$ coincide, Fig. 4(a) shows that $Q_{\text{abs}}^{\parallel} > Q_{\text{abs}}^{\perp}$ and $Q_{\text{abs}}^{\text{R}} \simeq Q_{\text{abs}}^{\text{L}}$ for all $k_0 c$. The excess of $Q_{\text{abs}}^{\parallel}$ over Q_{abs}^{\perp} increases with a rotation of $\underline{\underline{C}}$ about the z axis by $\alpha = 20^\circ$, as becomes evident from comparing Figs. 4(b) with 4(a), but $Q_{\text{abs}}^{\text{R}} \simeq Q_{\text{abs}}^{\text{L}}$ even for $\alpha = 20^\circ$. A subsequent rotation by $\beta = 40^\circ$ about the new y axis increases the excess of $Q_{\text{sca}}^{\text{R}}$ over $Q_{\text{sca}}^{\text{L}}$; see Fig. 4(c). This excess is not affected by a further rotation by $\gamma = 30^\circ$ about the latest z axis in Fig. 4(d). an additional conclusion is that $Q_{\text{abs}}^{\text{R}} - Q_{\text{abs}}^{\text{L}}$ is more sensitive than $Q_{\text{sca}}^{\text{R}} - Q_{\text{sca}}^{\text{L}}$ to the orientational mismatch of $\underline{\underline{C}}$ and $\underline{\underline{U}}$.

3.2 Rotation of $\underline{\underline{C}}$ about a shape principal axis

A general rotation of $\underline{\underline{C}}$, while keeping $\underline{\underline{U}}$ fixed, requires three consecutive rotations specified by Eq. (4). Each of those rotations has an effect on the scattering and absorption characteristics, as exemplified by Figs. 1 and 4. Therefore, we considered next the variation of Q_{sca} versus the angle of rotation, but for single rotations; i.e., Q_{sca} vs. α with $\beta = \gamma = 0^\circ$, and Q_{sca} vs. β with $\alpha = \gamma = 0^\circ$. In order to present salient features, we fixed $\varepsilon_r = 2$ and $\mu_r = 1.05$ for all results presented in this section; furthermore, as both $Q_{\text{sca}}^{\text{L}}$ and $Q_{\text{sca}}^{\text{R}}$ are then close to $(Q_{\text{sca}}^{\parallel} + Q_{\text{sca}}^{\perp})/2$, we restricted the incident plane wave to be linearly polarized.

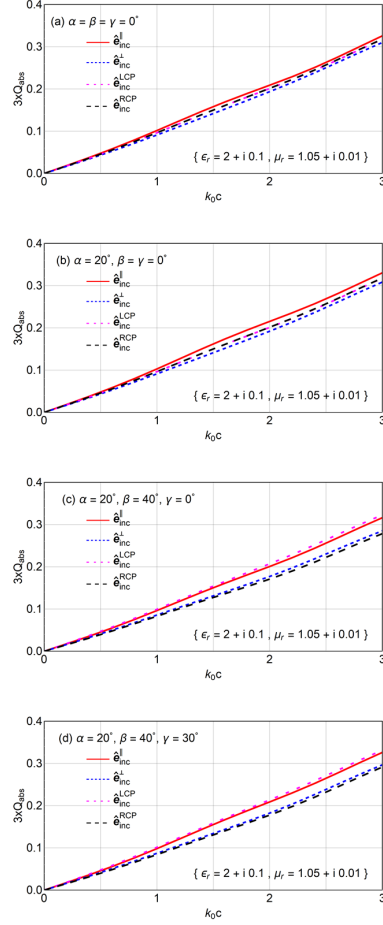


Figure 4: $Q_{\text{abs}}^{\parallel}$, Q_{abs}^{\perp} , $Q_{\text{abs}}^{\text{L}}$, and $Q_{\text{abs}}^{\text{R}}$ vs. $k_0 c \in [0, 3]$ for a biaxially dielectric-magnetic ellipsoid described by $\varepsilon_r = 2 + i0.1$, $\mu_r = 1.05 + i0.01$, $\alpha_x = 1.2$, $\alpha_y = 1.1$, $a/c = 1/2$, and $b/c = 2/3$. The angles of incidence are $\theta_{\text{inc}} = 45^\circ$ and $\phi_{\text{inc}} = 30^\circ$. (a) $\alpha = \beta = \gamma = 0^\circ$; (b) $\alpha = 20^\circ$ and $\beta = \gamma = 0^\circ$; (c) $\alpha = 20^\circ$, $\beta = 40^\circ$, and $\gamma = 0^\circ$; and (d) $\alpha = 20^\circ$, $\beta = 40^\circ$, and $\gamma = 30^\circ$.

In Figs. 5–9, results are presented for all six canonical configurations of the incident linearly polarized plane wave with respect to the semi-axes of the ellipsoid; i.e., $\hat{\mathbf{k}}_{\text{inc}} \in \{\hat{\mathbf{x}}, \hat{\mathbf{y}}, \hat{\mathbf{z}}\}$ and $\hat{\mathbf{e}}_{\text{inc}} \in \{\hat{\mathbf{x}}, \hat{\mathbf{y}}, \hat{\mathbf{z}}\}$ such that $\hat{\mathbf{k}}_{\text{inc}} \perp \hat{\mathbf{e}}_{\text{inc}}$.

Figure 5(a) shows plots of Q_{sca} vs. α when $\beta = \gamma = 0^\circ$ and Fig. 5(b) shows plots of Q_{sca} vs. β when $\alpha = \gamma = 0^\circ$, for a biaxially dielectric-magnetic ellipsoid when $\varepsilon_r = 2$, $\mu_r = 1.05$, $\alpha_x = 1.2$, $\alpha_y = 1.1$, $a/c = 1/2$, $b/c = 2/3$, and $k_0 c = 3$. Thus, the constitutive principal axes are rotated about the z axis of

the laboratory coordinate system for Fig. 5(a) and about the y axis of the laboratory coordinate system for Fig. 5(b).

When $\hat{\mathbf{k}}_{\text{inc}}$ is parallel to the axis of rotation, Q_{sca} has a very weak dependence on the rotation angle, as compared to when $\hat{\mathbf{k}}_{\text{inc}}$ is perpendicular to the axis of rotation. This characteristic is exemplified by

- the plots for $\hat{\mathbf{k}}_{\text{inc}} = \hat{\mathbf{z}}$ in comparison to those for $\hat{\mathbf{k}}_{\text{inc}} \in \{\hat{\mathbf{x}}, \hat{\mathbf{y}}\}$ in Fig. 5(a) as well as
- the plots for $\hat{\mathbf{k}}_{\text{inc}} = \hat{\mathbf{y}}$ in comparison to those for $\hat{\mathbf{k}}_{\text{inc}} \in \{\hat{\mathbf{x}}, \hat{\mathbf{z}}\}$ in Fig. 5(b).

This characteristic holds also for spheroids composed of the chosen material, as is evident from Fig. 6.

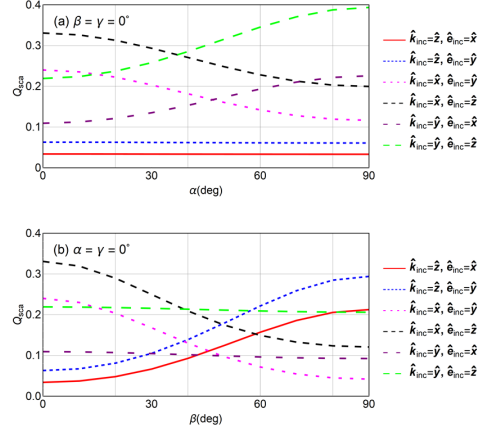


Figure 5: Q_{sca} vs. α and vs. β for a biaxially dielectric-magnetic ellipsoid when $\varepsilon_r = 2$, $\mu_r = 1.05$, $\alpha_x = 1.2$, $\alpha_y = 1.1$, $a/c = 1/2$, $b/c = 2/3$, and $k_0c = 3$. The constitutive principal axes are rotated about either (a) the z axis or (b) the y axis of the laboratory coordinate system.

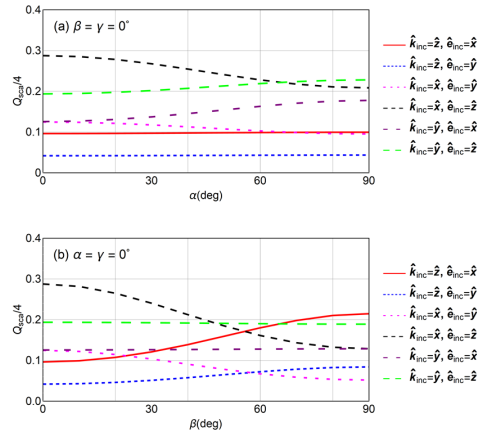


Figure 6: Same as Fig. 5, except for a spheroid ($a = c$, and $b = 2c/3$) when $k_0c = 2$.

Plots of Q_{sca} vs. α when $\beta = \gamma = 0^\circ$ or Q_{sca} vs. β when $\alpha = \gamma = 0^\circ$ in Figs. 5 and 6 can be predicted from plots of the scalar function

$$f(\alpha, \beta, \gamma) = \hat{\mathbf{k}}_{\text{inc}} \cdot \underline{\underline{C}}^{-1} \cdot \hat{\mathbf{k}}_{\text{inc}}, \quad (77)$$

vs. α when $\beta = \gamma = 0^\circ$ or vs. β when $\alpha = \gamma = 0^\circ$. These plots are shown in Fig. 7. When $f(\alpha, 0^\circ, 0^\circ)$ [or $f(0^\circ, \beta, 0^\circ)$] is invariant with respect to α (or β), Q_{sca} is weakly dependent on α (or β). Likewise, when $f(\alpha, 0^\circ, 0^\circ)$ [or $f(0^\circ, \beta, 0^\circ)$] increases/decreases as α (or β) increases, Q_{sca} also increases/decreases. Finally, when the value of $f(\alpha, 0^\circ, 0^\circ)$ [or $f(0^\circ, \beta, 0^\circ)$] is either a maximum or a minimum, the plot of Q_{sca} vs. α (or vs. β) also contains the same extremum. This is true regardless of k_0c , ε_r , μ_r , a/c , and b/c , as can be seen on comparing Figs. 5 and 6 with Fig. 7.

However, this prediction fails for compound rotations; e.g., the variation of Q_{sca} with respect to α is not predicted by the variation of $f(\alpha, \beta, \gamma)$ with respect to α when $\beta \neq 0^\circ$ and/or $\gamma \neq 0^\circ$. The failure is exemplified in Fig. 8 by a comparison of the plots of Q_{sca} and $f(\alpha, 40^\circ, 30^\circ)$ vs. α for the biaxially dielectric-magnetic ellipsoid of Fig. 5, but when $\beta = 40^\circ$ and $\gamma = 30^\circ$.

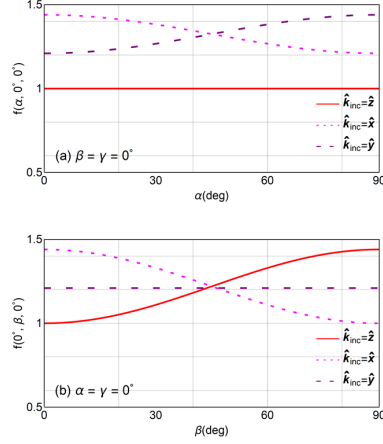


Figure 7: (a) $f(\alpha, 0^\circ, 0^\circ)$ vs. α and (b) $f(0^\circ, \beta, 0^\circ)$ vs. β , when $\alpha_x = 1.2$, and $\alpha_y = 1.1$.

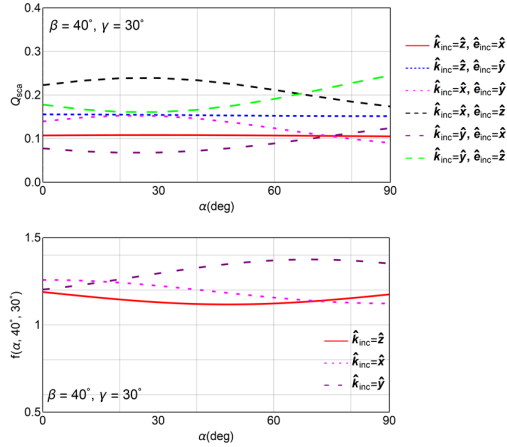


Figure 8: (Top) Q_{sca} vs. α for $\beta = 40^\circ$ and $\gamma = 30^\circ$ and (bottom) $f(\alpha, 40^\circ, 30^\circ)$ vs. α , when $\alpha_x = 1.2$ and $\alpha_y = 1.1$.

The foregoing investigation was repeated with the scattering material being dissipative, as in Sec. 3.3.1. The conclusions held for Q_{sca} . However, neither the variation of Q_{abs} with α could be predicted from $f(\alpha, 0^\circ, 0^\circ)$ nor the variation of Q_{abs} with β could be predicted from $f(0^\circ, \beta, 0^\circ)$.

The shape effect can also be appreciated by comparisons with a sphere. Figure 9(a) shows plots of Q_{sca}

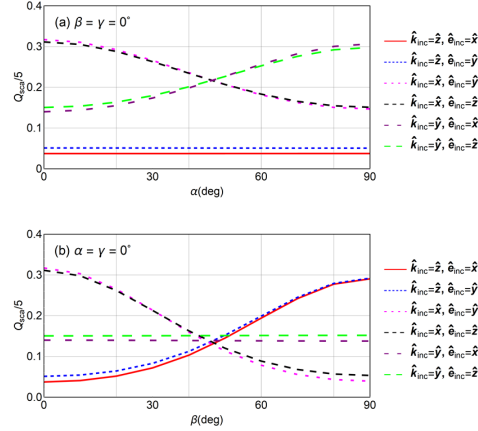


Figure 9: Same as Fig. 5, except for a sphere ($a = b = c$).

vs. α , and Fig. 9(b) shows plots of Q_{sca} vs. β , both when $a = b = c$. For fixed $\hat{\mathbf{k}}_{\text{inc}}$, $\hat{\mathbf{e}}_{\text{inc}}$ has a noticeable effect on the curves of Q_{sca} vs. α , as well as on Q_{sca} vs. β when $a \neq b \neq c$ compared to when $a = b = c$. For example, the curves of Q_{sca} vs. α for

- $\{\hat{\mathbf{k}}_{\text{inc}} = \hat{\mathbf{x}}, \hat{\mathbf{e}}_{\text{inc}} = \hat{\mathbf{y}}\}$ and
- $\{\hat{\mathbf{k}}_{\text{inc}} = \hat{\mathbf{x}}, \hat{\mathbf{e}}_{\text{inc}} = \hat{\mathbf{z}}\}$

are very close to each other when $a = b = c$ [Fig. 9(a)] but not when $a \neq b \neq c$ [Fig. 5(a)]. When the same exercise was conducted with the scattering material being dissipative, the conclusion was found to hold for both Q_{sca} and Q_{abs} .

4 Concluding Remarks

We derived expressions of the vector spherical wavefunctions for an orthorhombic dielectric-magnetic material with a permeability dyadic that is a scalar multiple of the permittivity dyadic and with constitutive principal axes that are arbitrarily oriented in the laboratory coordinate system. These expressions were used in formulating the extended boundary condition method for scattering by a three-dimensional object composed of the chosen material. Numerical results were obtained for plane-wave scattering by an ellipsoid composed of the chosen material, and the effect of the rotation of the constitutive principal axes relative to the shape principal axes was studied.

The following conclusions were drawn from the numerical results obtained by us:

- The difference between $Q_{\text{sca}}^{\parallel}$ and Q_{sca}^{\perp} is much larger than the difference between $Q_{\text{sca}}^{\text{L}}$ and $Q_{\text{sca}}^{\text{R}}$. The difference between $Q_{\text{sca}}^{\text{L}}$ and $Q_{\text{sca}}^{\text{R}}$ increases as the orientational mismatch between the constitutive principal axes and the shape principal axes becomes more pronounced and/or the electrical size of the ellipsoid increases.
- The difference between $Q_{\text{abs}}^{\parallel}$ and Q_{abs}^{\perp} is much larger than the difference between $Q_{\text{abs}}^{\text{L}}$ and $Q_{\text{abs}}^{\text{R}}$, if the scattering material is dissipative. The difference between $Q_{\text{abs}}^{\text{L}}$ and $Q_{\text{abs}}^{\text{R}}$ increases as the orientational mismatch between the constitutive principal axes and the shape principal axes becomes more pronounced and/or the electrical size of the ellipsoid increases.
- When the scattering material is impedance-matched (i.e., $\varepsilon_r = \mu_r$) to the surrounding free space, the differential scattering efficiency does not depend on the polarization state of the incident plane wave,

regardless of the orientational mismatch between the constitutive principal axes and the shape principal axes. This independence extends to the total scattering, extinction, and absorption efficiencies as well.

- The dependence of Q_{sca} on the angle of rotation about a shape principal axis can be predicted qualitatively from the variation of the scalar $\hat{\mathbf{k}}_{\text{inc}} \cdot \underline{\underline{C}} \cdot \hat{\mathbf{k}}_{\text{inc}}$ with respect to the angle of rotation, regardless of ε_r , μ_r , a/c , b/c , and k_0c . When $\hat{\mathbf{k}}_{\text{inc}}$ is parallel to the axis of rotation, Q_{sca} does not vary considerably with respect to the angle of rotation, as compared to when $\hat{\mathbf{k}}_{\text{inc}}$ is perpendicular to that axis.
- When the scattering material is nondissipative, Q_{sca} is maximum when both ε_r and μ_r are negative, intermediate when the two have opposite signs, and minimum when both are positive, regardless of the orientational mismatch between the constitutive principal axes and the shape principal axes.
- Both Q_{sca} and Q_{abs} are more sensitive to the polarization state of the incident plane wave for ellipsoids and spheroids than for spheres.

Acknowledgment. AL thanks the Charles Godfrey Binder Endowment at Penn State for ongoing support of his research activities. The authors are grateful to an anonymous reviewer for comments that led to improved presentation.

References

- [1] E. J. Post, *Formal Structure of Electromagnetics* (North-Holland, 1962).
- [2] T. G. Mackay and A. Lakhtakia, *Electromagnetic Anisotropy and Bianisotropy: A Field Guide* (World Scientific, 2010).
- [3] H. C. Chen, *Theory of Electromagnetic Waves* (McGraw–Hill, 1983).
- [4] M. V. Berry, “The optical singularities of bianisotropic crystals,” *Proc. R. Soc. Lond. A* **461**, 2071–2098 (2005).
- [5] R. E. Collin, *Field Theory of Guided Waves* (IEEE Press, 1991).
- [6] M. Faryad and A. Lakhtakia, *Infinite-Space Dyadic Green Functions in Electromagnetism* (Morgan & Claypool, 2018).
- [7] A. Lakhtakia and T. G. Mackay, “Vector spherical wavefunctions for orthorhombic dielectric-magnetic material with gyrotropic-like magnetoelectric properties,” *J. Opt. (India)* **41**, 201–213 (2012).
- [8] P. C. Waterman, “Matrix formulation of electromagnetic scattering,” *Proc. IEEE* **53**, 805–812 (1965).
- [9] A. Lakhtakia, “The Ewald–Oseen extinction theorem and the extended boundary condition method,” in *The World of Applied Electromagnetics*, A. Lakhtakia and C. M. Furse, eds. (Springer, 2018), pp. 481–513.
- [10] P. M. Morse and H. Feshbach, *Methods of Theoretical Physics, Vol. II* (McGraw–Hill, 1953), pp. 1865–1866.
- [11] P. Barber and C. Yeh, “Scattering of electromagnetic waves by arbitrarily shaped dielectric bodies,” *Appl. Opt.* **14**, 2864–2872 (1975).
- [12] H. Lütkepohl, *Handbook of Matrices* (Wiley, 1996).
- [13] K. W. Whites and C. Y. Chung, “Composite uniaxial bianisotropic chiral materials characterization: Comparison of predicted and measured scattering,” *J. Electromagn. Waves Appl.* **11**, 371–394 (1997).

- [14] T. G. Mackay and W. S. Weiglhofer, “Homogenization of biaxial composite materials: bianisotropic properties,” *J. Opt. A: Pure Appl. Opt.* **3**, 45–52 (2000).
- [15] R. Marqués, F. Medina, and R. Rafi-El-Idrissi, “Role of bianisotropy in negative permeability and left-handed metamaterials,” *Phys. Rev. B* **65**, 144440 (2002).
- [16] S. N. Sheikholeslami, H. Alaeian, A. L. Koh, and J. A. Dionne, “A metafluid exhibiting strong optical magnetism,” *Nano Lett.* **13**, 4137–4141 (2013).
- [17] J. Plébanski, “Electromagnetic waves in gravitational fields,” *Phys. Rev.* **118**, 1396–1408 (1960).
- [18] C. F. Bohren and D. R. Huffman, *Absorption and Scattering of Light by Small Particles* (Wiley, 1983).
- [19] H. M. Alkhoori, A. Lakhtakia, J. K. Breakall, and C. F. Bohren, “Plane-wave scattering by an ellipsoid composed of an orthorhombic dielectric–magnetic material,” *J. Opt. Soc. Am. A* **35**, 1549–1559 (2018).
- [20] K. Aydin and A. Hizal, “On the completeness of the spherical vector wave functions,” *J. Math. Anal. Appl.* **117**, 428–440 (1986).
- [21] J. A. Stratton, *Electromagnetic Theory* (McGraw–Hill, 1941), pp. 564–565.
- [22] J. J. Bowman, T. B. A. Senior, and P. L. E. Uslenghi, eds., *Electromagnetic and Acoustic Scattering by Simple Shapes* (North-Holland, 1969).
- [23] M. A. Karam and A. K. Fung, “Vector forward scattering theorem,” *Radio Sci.* **17**, 752–756 (1982).
- [24] C. E. Baum, “The forward-scattering theorem applied to the scattering dyadic,” *IEEE Transactions on Antennas and Propagation* **55**, 1488–1494 (2007).
- [25] H. M. Alkhoori, A. Lakhtakia, J. K. Breakall and C. F. Bohren, “Scattering by a three-dimensional object composed of the simplest Lorentz-nonreciprocal medium,” *J. Opt. Soc. Am. A* **35**, 2026–2034 (2018).
- [26] Y. Jaluria, *Computer Methods for Engineering* (Taylor & Francis, 1996), Sec. 7.5.3.
- [27] I. S. Gradshteyn and I. M. Ryzhik, *Table of Integrals, Series, and Products* 7th edn. (Academic Press, 2007).
- [28] E. Kreyszig, *Advanced Engineering Mathematics* 10th edn. (Wiley, 2011), Sec. 20.2.
- [29] A. D. U. Jafri and A. Lakhtakia, “Scattering of an electromagnetic plane wave by a homogeneous sphere made of an orthorhombic dielectric-magnetic material,” *J. Opt. Soc. Am. A* **31**, 89–100 (2014).
- [30] A. D. U. Jafri and A. Lakhtakia, “Scattering of an electromagnetic plane wave by a homogeneous sphere made of an orthorhombic dielectric-magnetic material: erratum,” *J. Opt. Soc. Am. A* **31**, 2630 (2014).
- [31] P. W. Barber and S. C. Hill, *Light Scattering by Particles: Computational Methods* (World Scientific, 1990).